Pergamon

Int. J. Heat Mass Transfer. Vol. 40, No. 2, pp. 407–419, 1997

0017–9310/97 $15.00+0.00

PII: S0017-9310(96)00068-3

Thermoacoustic waves in a confined medium

YUFENG HUANG and HAIM H. BAU†

Department of Mechanical Engineering and Applied Mechanics, University of Pennsylvania, Philadelphia, PA 19104-6315, U.S.A.

(*Received* 14 *April* 1995 *and in final form* 5 *February* 1996)

Abstract—The generation and transmission of linear and nonlinear thermoacoustic (TAC) waves in a confined gaseous medium, with a Prandtl number of 3/4, are investigated theoretically. The linearized equations are solved using the Laplace transform method with numerical inversion to obtain the pressure and temperature distributions in the cavity and the wall heat flux for various wall heating conditions. The nonlinear equations are solved accurately with finite differences. The differences between the linear and nonlinear waves are delineated. During the expansion phase, the nonlinear wave temperature dips below the average medium temperature. This cooling phenomenon is not exhibited by linear waves. The theoretical predictions are critically compared with Brown and Churchill's experimental observations from 1995.

1. INTRODUCTION

We study the generation and transmission of thermoacoustic (TAC) waves in a gas-filled, one-dimensional cavity of length L^*. The temperature of the left hand side (LHS) wall is rapidly changed, while the opposite [right hand side (RHS)] wall temperature is maintained fixed. As a result of the LHS wall's temperature increase, a sudden expansion of the adjacent gas occurs, which in turn generates a pressure wave. This thermally-induced wave propagates at approximately the speed of sound (a_0^*) in the medium and bounces off the opposite wall. The wave travels back towards the hot wall and gets reflected again. Numerous reflections with a frequency, $f^* \sim a_0^*/2L^*$, occur until the wave eventually damps out because of heat and viscous dissipation.

In Huang and Bau [1], we investigated the generation and transmission of linear and nonlinear TAC waves in a semi-infinite medium and provided an extensive review of the pertinent literature on TAC waves, which for brevity's sake we will not repeat here. We mention below only the most relevant studies to our current investigation.

There are only a few experimental studies that focus on TAC waves. At a point inside a closed cylinder, one end of which was subjected to a sudden temperature change, Parang and Salah-Eddine [2] measured the temperature as a function of time and demonstrated that TAC waves enhance mixing. Brown [3] and Brown and Churchill [4, 5] measured pressure as a function of time. However, no direct measurements of heat transfer were made.

Numerical studies of one and two-dimensional TAC waves in a confined region have been carried out by Brown [3], Larkin [6], Spradley and Churchill [7] and Ozoe *et al.* [8, 9]. All these investigators solved numerically the compressible Navier–Stokes equations for a gas with temperature-independent thermophysical properties using finite differences, with the convective derivatives being approximated by a first-order upwinding scheme. They employed a relatively crude grid spacing which may have adversely affected the precision of their results. Indeed, as Brown [3] noted, the aforementioned numerical results do not resemble his experimental observations.

Huang and Bau [1] solved the linearized equations for TAC waves in a semi-infinite medium using a numerical inverse transform (ILT) method. The method was verified by comparing the numerical results with asymptotic ones and with experimental data, which was demonstrated to be highly accurate. They also solved the nonlinear equations in a semi-infinite medium using a high order, finite difference technique employing very fine spatial and time steps. The adequacy of the grid spacing was validated by comparing the code predictions for linear waves with the ones obtained using the ILT method.

In this paper, we first study the transmission of linear waves in a cavity subjected to a timewise step change in the wall temperature. Then we examine the effect of gradual wall heating on the characteristics of the linear TAC waves. Subsequently, using finite differences with fine grid spacing, we compute the nonlinear waves with temperature dependent thermophysical properties. We compare our results to those obtained by Vasilyev and Paolucci [10], who developed a novel wavelet transform numerical technique. Finally, we compare our theoretical results with the experimental observations of Brown [3].

The motivation for this study is our desire to better understand the contribution of TAC waves to the heat

† Author to whom correspondence should be addressed.

NOMENCLATURE

a	speed of sound
A	the magnitude of the change in the wall temperature
f	frequency
L	cavity's length
P	pressure
q	wall heat flux
Pr	Prandtl number
R	ideal gas constant
t	time
t_0	time required for the wave to travel the cavity's length
T	temperature
T_w	heated wall temperature
V	velocity
y	distance from the heated wall.

Greek symbols

α	thermal diffusivity
τ	time delay
μ	dynamic viscosity
γ	ratio of specific heats
ρ	density.

Superscripts

$\hat{}$	quantities normalized with cavity variables
*	dimensional quantities.

Subscripts

0	quiescent conditions

Abbreviations

ILT	inverse laplace transform
FD	finite differences
TAC waves	thermoacoustic waves.

transfer process and, more specifically, to explore the possible role of TAC waves in two particular, instrumentation-related applications. First of all, we are interested in the potential use of thermal actuators for the generation of acoustic waves. When one of the cavity walls is made out of a flexible membrane, the bouncing back and forth of the TAC wave inside the cavity will cause the membrane to vibrate and radiate acoustic waves outside the cavity. In other words, the device can work as a 'thermal loud speaker'.

Secondly, we wish to evaluate the contribution of TAC waves to noise problems which adversely affect the performance of thermal conductivity detectors used in chromatography to measure the concentration of flowing gases. These sensors typically consist of a constant temperature filament embedded in a constant, lower temperature channel. The thermal conductivity of the gas is inferred from the filament's power consumption. When the colder gas encounters the hot filament, a sudden expansion of the gas occurs which, in turn, induces TAC waves. These waves bounce back and forth between the filament and the cold walls, inducing fluctuations in the power dissipated from the filament. This time-dependent heat transfer is interpreted by the sensor as noise, and it adversely impacts the sensor's sensitivity. Before addressing the somewhat more difficult problems of TAC waves in a moving gas and in the presence of moving boundaries, we study here the simpler problem of TAC waves in a quiescent medium confined in a cavity with perfectly rigid boundaries.

2. MATHEMATICAL MODEL

Consider initially quiescent, compressible gas at a uniform pressure (P_0^*) and temperature (T_0^*) confined between two rigid, parallel walls placed distance L^* apart. Properties corresponding to the quiescent, initial state are denoted by a subscript zero. The temperature, $T_w^*(t)$, of the left solid wall is suddenly increased, while the temperature of the right wall is maintained for all times at the initial gas temperature (T_0^*). As a result of the left wall's temperature alteration, a pressure wave is generated in the gas near the heated wall and propagates away from the wall in the positive (y) direction. Once the wave reaches the right, cold wall, it bounces off it and propagates in the negative y direction. The wave will undergo numerous reflections until eventually it damps out due to viscous and thermal dissipation.

The nondimensional continuity, momentum, energy and state equations for one-dimensional TAC waves were given in ref. [1]. The boundary and initial conditions for the confined case are

$$T(0,t) - T_w(t) = V(0,t) = T(L,t) = V(L,t) = 0 \tag{1}$$

and

$$T(y,0) = \frac{\partial T}{\partial t}(y,0) = V(y,0) = \frac{\partial V}{\partial t}(y,0) = 0. \tag{2}$$

In the above, V, P and T are, respectively, the

velocity, pressure and temperature deviations from the corresponding quiescent values. P_0^*, T_0^* and ρ_0^* are, respectively, the pressure, temperature and density scales. All variables with and without a superscript (*) are, respectively, dimensional and nondimensional. The sound speed in the undisturbed gas, $a_0^* = \sqrt{\gamma R^* T_0^*}$, is the velocity scale. R^* is the gas constant. $\gamma = C_p^*/C_v^*$ is the ratio of the specific heats, which we assumed to be temperature-independent. The length scale is, $(4/3)\gamma(\mu_0^*/\rho_0^* a_0^*)$ where μ_0^* is the viscosity and $(4/3)\gamma(\mu_0^*/\rho_0^*(a_0^*)^2)$ is the time scale. We neglected buoyancy since, even if buoyant forces were present, the time-scale associated with the buoyant flow would be much larger than that of the acoustic wave [7]. We approximated the nondimensional viscosity and thermal conductivity by $\mu(T) = \mu_1\sqrt{1+T}+\mu_2$ and $k(T) = k_1\sqrt{1+T}+k_2$, where $\mu_1+\mu_2 = 1$ and $k_1+k_2 = 1$. Unless otherwise stated, our results are presented for $Pr = 3/4$, $\gamma = 1.4$, $\mu_1 = 1.489$ and $k_1 = 1.66$. This data corresponds, approximately, to nitrogen at $T_0^* = 300\,\mathrm{K}$.

The linear equations were solved using the Laplace transform method (ILT). Unfortunately, analytic inversion is not feasible. Instead, we used the FORTRAN routine ACM-Alg. 219 [11] to obtain the inversion integrals numerically. The ILT has the advantage that it allows one to compute the required variables at any location and at any time without having to compute the entire flow field, as would be the case if one were to use finite differences or elements. By comparing the numerical inversion's results with analytic long time asymptotes, Huang and Bau found this technique to be highly accurate and free of the numerical dissipation which plagued many other numerical schemes (see, for example, Brown [3]).

The nonlinear equations were solved using a finite differences, implicit, Crank–Nicolson scheme modified with a Galerkin finite element interpolation in space [12]. The convective derivates were approximated with a truncation error $O(\Delta t^2, \Delta y^4)$, where Δy and Δt are, respectively, space and time steps. The diffusive terms were approximated using central differences to $O(\Delta y^2)$. Thus, the scheme was $O(\Delta^2, \Delta y^2)$ accurate. Below, we refer to this scheme as FD.

The grid spacing in FD required to achieve the desired precision was determined by verifying that, in the framework of the L^2 norm, the FD predictions for linear waves deviated by less than 0.01% from the highly accurate ILT solutions. In the case of the semi-infinite medium, the nonlinear FD predictions also agreed well with solutions obtained with a finite element code (see ref. [1]). Additionally, the nonlinear solutions demonstrated grid-size independence. Finally, in Section 5, we obtained an excellent agreement between our nonlinear FD simulations and recent results obtained with the wavelet transform method [10]. Further details on the verification and performance of the FD scheme are available in refs. [1, 13].

3. LINEAR TAC WAVES GENERATED BY A STEP CHANGE IN THE WALL TEMPERATURE

In this section, we investigate TAC waves generated by a step change in the wall's temperature

$$T_w(t) = \begin{cases} 0 \text{ for } t \leqslant 0 \\ A \text{ for } t > 0 \end{cases}. \tag{3}$$

The linear results were obtained with the ILT scheme. We find it convenient to present the results of our calculations in terms of the normalized distance $\hat{y} = y/L$ $(0 \leqslant \hat{y} \leqslant 1)$ and the normalized time, $\hat{t} = t/t_0$, where $t_0 = L$ represents the nondimensional time it takes the linear wave to travel the length of the cavity. All the calculations were carried out for a cavity of length $L = 13\,000$. The pressure wave hits the cold wall at $\hat{t} \sim (2n+1)$, where $n = 0, 1, 2, \ldots$ is an integer.

At times $\hat{t} = 0.25$, 1, 1.5 and 2. Fig. 1 depicts the linear pressure wave (solid lines) as a function of $\hat{y}$. The arrows in the figure indicate the direction of the wave motion. The pressure wave is characterized by a sharp front and a long tail. As time goes by, as a result of molecular diffusion, the width of the peak broadens and its height decreases. When the pressure wave encounters solid walls, it gets reflected and its amplitude increases. This increase is a result of the reflected wave being superimposed on the incident wave. The average temperature of the gas in the cavity increases gradually. This, in turn, causes an increase in the cavity's mean pressure. The pressure wave is superimposed on this mean value. Eventually, the average pressure reaches the asymptotic value of 0.5, which corresponds to a linear, steady-state, conductive temperature profile. For example, when the gas is nitrogen initially at STP and the dimensional length of the cavity $L^* = 1$ mm, the linear wave peak $P/A \cong 0.1(\sim 33\ \mathrm{Pa\ K^{-1}})$ at $t^* \sim 2.8\ \mu\mathrm{s}$.

Figure 2 depicts the linear pressure wave fluctuations at the cold wall $(\hat{y} = 1)$ as a function of the normalized time, $\hat{t}$. The wave resonates in the cavity at a nondimensional frequency, $\hat{f} \sim 1/2$, which corresponds to a dimensional frequency, $f^* \sim a_0^*/2L^*$. For example for nitrogen at STP in a 1 mm wide box, $f^* \sim 170$ kHz. As $\hat{t}$ increases, the wave peak broadens (a feature which is somewhat obscured in Fig. 2 due to the logarithmic time scale), and its amplitude decreases due to a loss of energy. The pressure oscillations persist around the mean pressure in the cavity for the entire time interval depicted in Fig. 2. However, for times $\hat{t} > 300$, these oscillations are no longer visible on the scale of the figure. In order to be able to see these oscillations, the vertical scale of the figure must be magnified, as we have done in the insert of $300 < \hat{t} < 306$. The rate of decay of the pressure wave's amplitude in the confined medium is faster than in the semi-infinite domain (see ref. [13] for further details). This can be attributed, in part, to heat losses to the cold wall and the increased dissipation due to the increases in the wave's amplitude upon reflections from the solid walls.

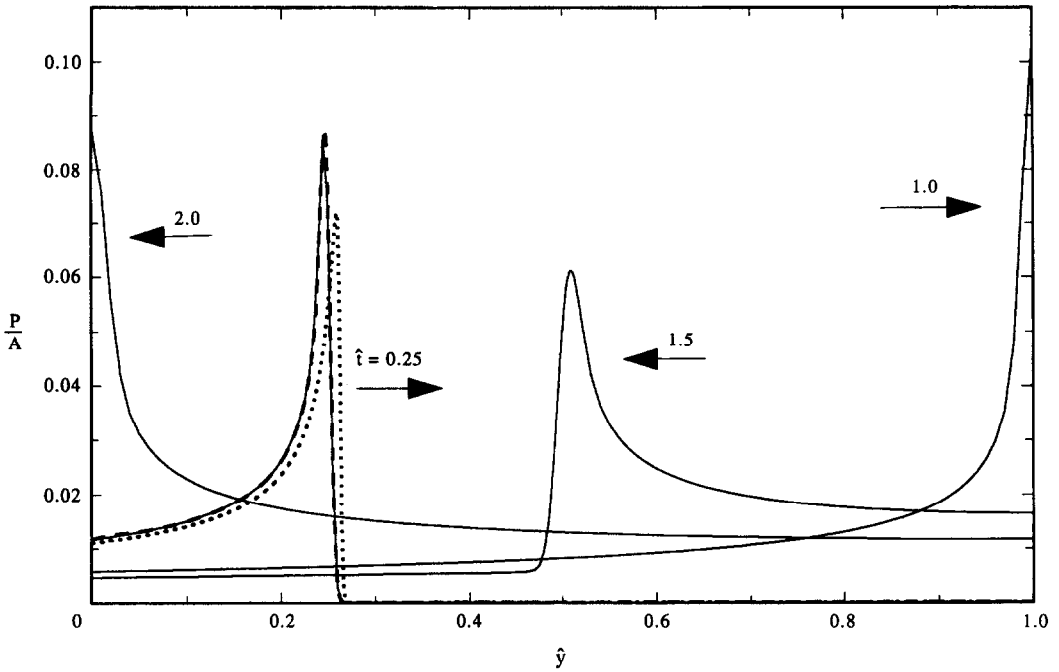

Fig. 1. At normalized times $\hat{t} = 0.25$, 1, 1.5 and 2, the pressure is depicted as a function of the normalized coordinate $\hat{y}$. $\tau = 0$. $L = 13000$. The solid, dashed and dotted lines represent, respectively, linear (ILT), linear (FD) and nonlinear (FD) waves with $A = 1$.

For $\hat{t} = 0.5$, 1.0, 1.5 and 2, Fig. 3 depicts the velocity (V/A) of the linear wave (solid lines) as a function of $\hat{y}$. Like the pressure wave, the velocity wave is characterized by a sharp front and a relatively long tail. For $\hat{t} > 1$, consistent with a compression wave, the gas flow is always directed towards the peak. For example, for $\hat{t} = 1.5$, $V < 0 (V > 0)$ to the right (left) of the peak. In other words, the gas in front of the peak moves in a direction opposite to that of the wave.

At $\hat{t} = 10.5$, Fig. 4 depicts the temperature and pressure distributions in the cavity as functions of $\hat{y}$. Figure 4 also shows the temperature distribution resulting from conduction in an incompressible medium. The TAC temperature distribution is characterized by two

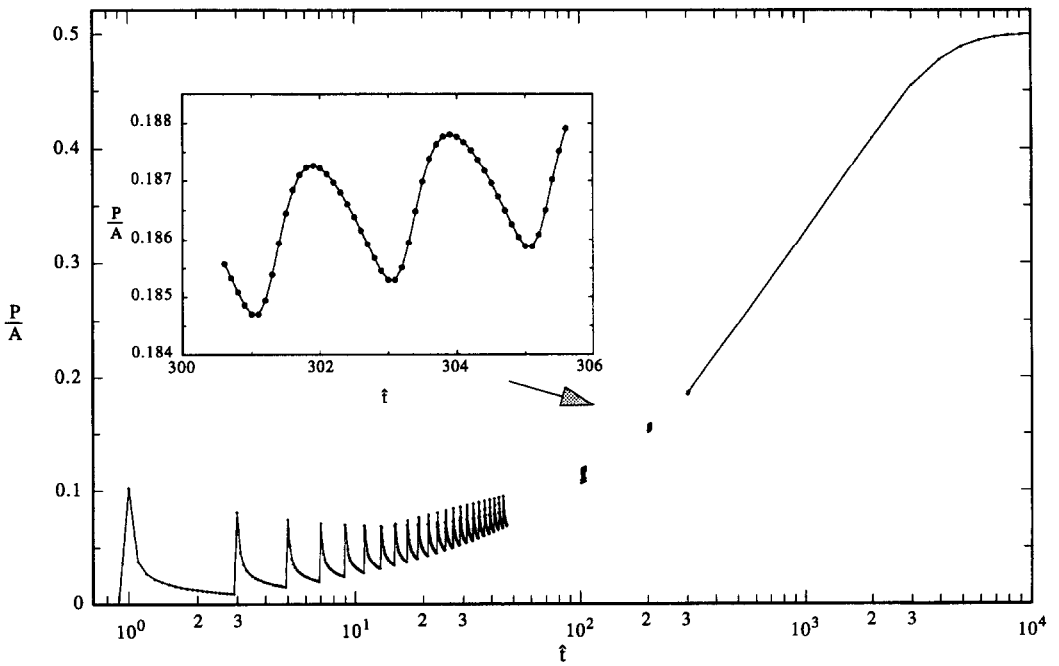

Fig. 2. The linear pressure at the cold wall ($\hat{y} = 1$) is depicted as a function of the normalized time, $\hat{t}$. $\tau = 0$. $L = 13000$.

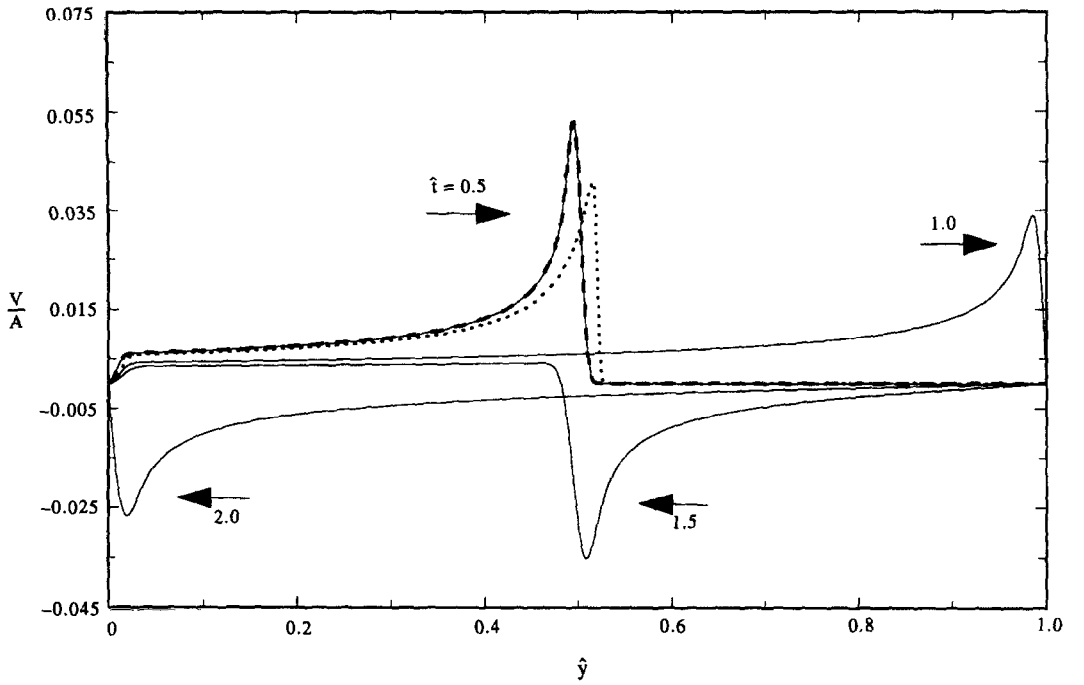

Fig. 3. At normalized times $\hat{t} = 0.5$, 1, 1.5 and 2, the linear (solid line, ILT, dashed line, FD) and the nonlinear (dotted line, FD, $A = 1$) velocities, V, are depicted as functions of the normalized coordinate $\hat{y}$. $\tau = 0$. $L = 13\,000$.

boundary layers at the hot and cold walls. At the hot wall, the temperature declines quickly from the value of A to about $0.01A$. When the gas thermal expansion is accounted for, the thickness of the hot thermal boundary layer is slightly smaller than the conductive boundary layer thickness of about $\sqrt{\alpha^* t^*}$. This is because of the conversion of thermal energy into pressure work. This effect is caused by the medium's com-

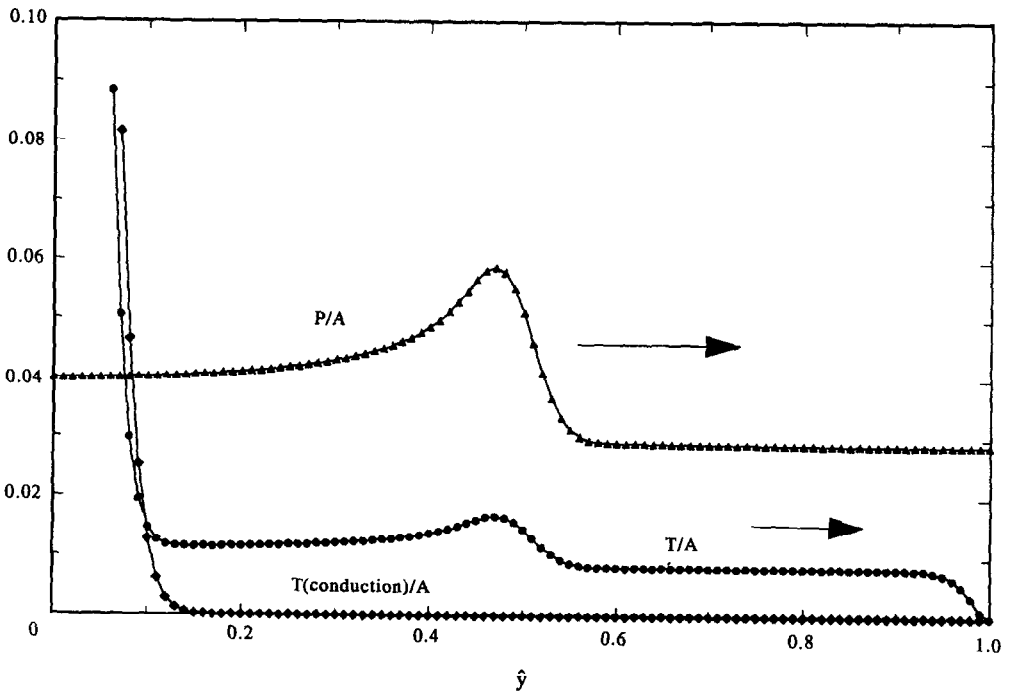

Fig. 4. At normalized time $\hat{t} = 10.5$, the linear pressure, the linear temperature in the presence of TAC waves, and the incompressible conductive temperature distributions are depicted as functions of the normalized coordinate $\hat{y}$. $\tau = 0$. $L = 13\,000$.

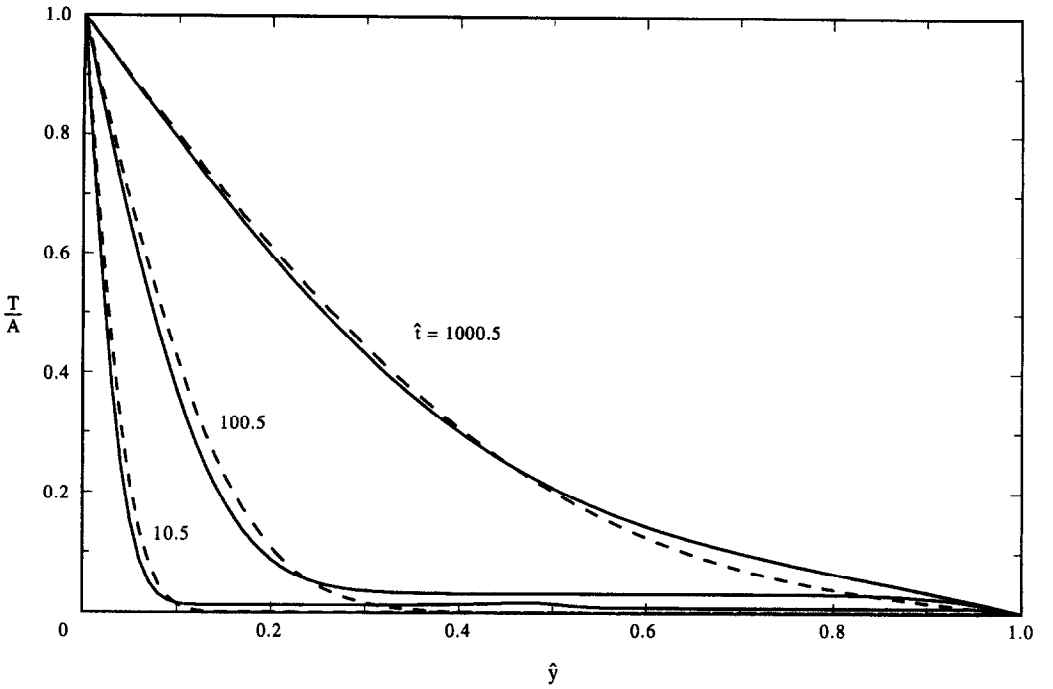

Fig. 5. At normalized times $\hat{t} = 10.5$, 100.5 and 1000.5, the linear temperature distribution is depicted as a function of the normalized coordinate $\hat{y}$. $\tau = 0$. $L = 13\,000$. The solid and dashed lines correspond, respectively, to temperature distributions in the presence and absence (conduction only) of TAC waves.

pressibility, and it is present even in the absence of TAC waves. A second boundary layer is formed next to the cold wali, where the temperature declines from 0.01 A to 0. In Fig. 4, the temperature assumes a local peak at the same location, $\hat{y} \sim 0.5$, where the pressure has its peak. The temperature peak is a result of the nearly adiabatic compression process.

For $\hat{t} = 10.5$, 100.5 and 1000.5, Fig. 5 depicts the temperature, T/A, as a function of $\hat{y}$ in the presence (solid line) and absence of TAC waves (conduction in an incompressible medium, dashed lines). When gas compressibility is accounted for, the temperature profile has a higher gradient at the hot wall, which indicates a slightly higher heat transport rate. The TAC waves also tend to increase slightly the temperature in the vicinity of the cold wall.

The effect of the linear TAC wave on the nondimensional heat flux (q/A) at the hot and cold walls as a function of time is shown, respectively, in Figs. 6 and 7 ($\tau = 0$). The heat flux is scaled with

$$\frac{k_0^* T_0^*}{\frac{4}{3}\gamma \frac{\mu_0^*}{a_0^* \rho_0^*}}.$$

The light and heavy solid lines ($\tau = 0$) in Fig. 6 correspond, respectively, to the flux in the presence of TAC waves and in the presence of conduction alone (in an incompressible medium). In Fig. 6, the dips in the solid line at $\hat{t} \sim 2n$, where $n \geqslant 1$ is an integer, correspond to the times when the pressure wave arrives at the hot wall. When the compression wave hits the hot wall, the gas' temperature increases and its ability to absorb heat from the wall decreases. Excluding the dips, the heat flux in the compressible medium is $\sqrt{\gamma}$ times the heat flux in the presence of incompressible conduction alone. This augmentation in the heat transfer is due to the medium's compressibility, and it is not a direct result of the TAC wave.

In Fig. 7, the peaks in the heat flux (dotted line, $\tau = 0$) are a result of the increased temperature of the gas in the vicinity of the cold wall caused by the compression wave when it arrives at the wall times, $\hat{t} \sim (2n-1)$, where $n \geqslant 1$ is an integer. The conductive heat flux is not shown, since for the time interval depicted in Fig. 7 it has not yet penetrated as far as the cold wall.

4. THE EFFECT OF THE WALL HEATING RATE ($\tau > 0$)

Thus far, we have considered the idealized TAC waves generated by a step change in the wall temperature. In practice, as a result of the wall's and/or heater's thermal inertia and heat losses to the environment, it is not possible to generate a step change in the wall's temperature. We, therefore, approximate the dependence of the wall temperature on time by the simplified exponential expression,

$$T_w(t) = A\left(1 - \exp\left(-\frac{t}{\tau}\right)\right), \tag{4}$$

where τ is the time constant of the heating process. A

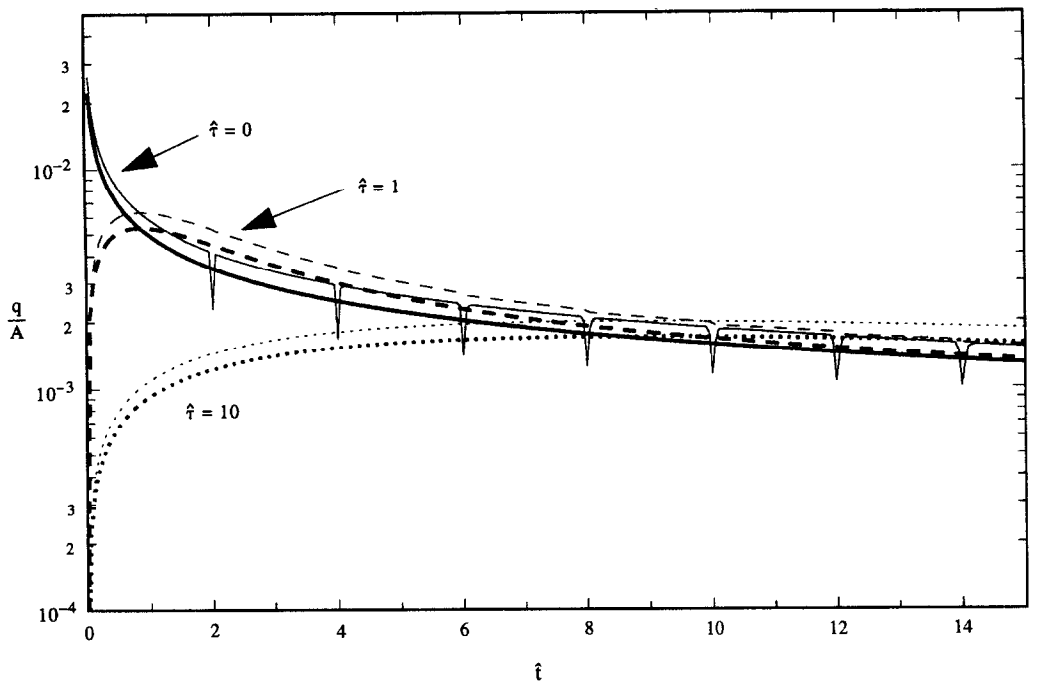

Fig. 6. For $\hat{\tau} = 0$, 1 and 10, the linear heat flux at the hot wall ($\hat{y} = 0$) is depicted as a function of the normalized time, $\hat{t}$. The light and dark lines correspond, respectively, to heat fluxes in the presence and absence (conduction only) of TAC waves. $L = 13\,000$.

step change in the wall's temperature corresponds to $\tau = 0$.

The effect of the normalized time constant $\hat{\tau} = \tau/t_0$ on the shape of the pressure wave is illustrated in Fig. 8, which depicts the pressure at the cold wall ($\hat{y} = 1$) as a function of time $\hat{t}$ for $\hat{\tau} = 0$, 0.2, 1 and 10. As $\hat{\tau}$ increases, the magnitude of the pressure peak decreases and its width increases. For $\hat{\tau} \sim 10$, there

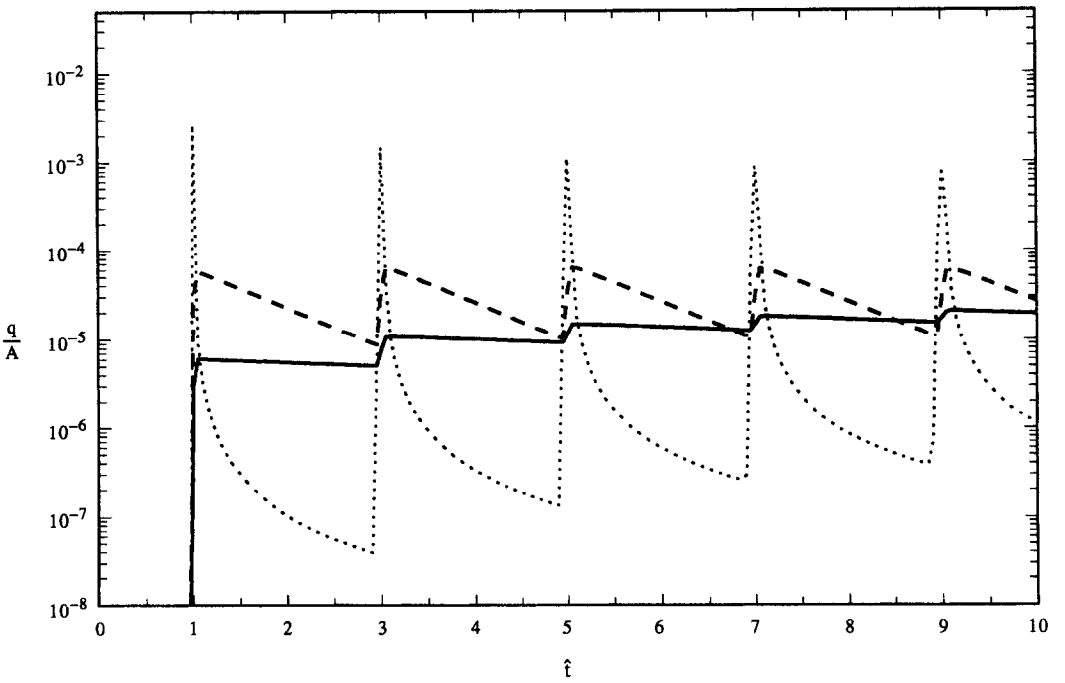

Fig. 7. For $\hat{\tau} = 0$, 1 and 10, the linear heat flux at the cold wall ($\hat{y} = 1$) is depicted as a function of the normalized time, $\hat{t}$. $L = 13\,000$.

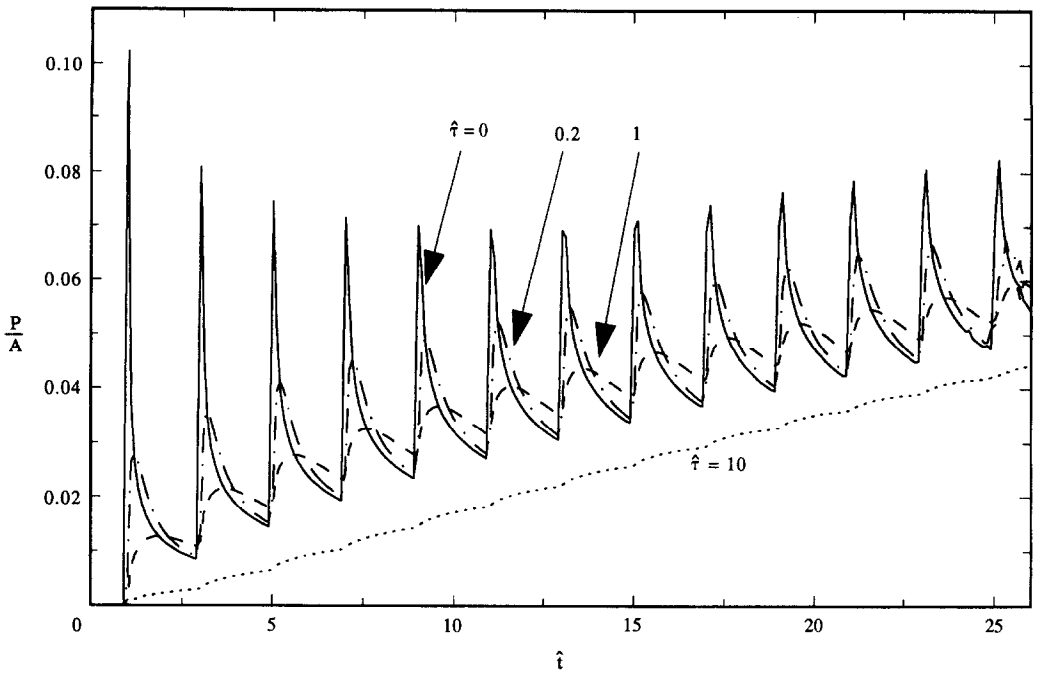

Fig. 8. For $\hat{\tau} = 0$, 0.2, 1 and 10, the linear pressure at the cold wall ($\hat{y} = 1$) is depicted as a function of the normalized time, $\hat{t}$. $L = 13\,000$.

are almost no visible oscillations. Thus, in order to generate appreciable pressure waves in a cavity, the time constant associated with the heating process must be sufficiently smaller than the time it takes the acoustic wave to traverse the width of the cavity. As t/τ increases, the difference between the pressure waves generated by sudden ($\tau = 0$) and gradual ($\tau > 0$) increases in the wall's temperature diminishes.

The effect of $\hat{\tau}$ on the hot wall ($\hat{y} = 0$) heat flux (q/A) is illustrated in Fig. 6. For $\hat{\tau} = 0$, 1, and 10, the figure depicts $q(t)/A$ in the presence of TAC waves (thin lines) and in the presence of conduction in an incompressible medium (thick lines) as functions of $\hat{t}$. Because of the conversion of heat into work, the heat flux in the compressible medium always exceeds that in the incompressible medium. For the physically unrealistic case of a step change in the wall temperature ($\hat{\tau} = 0$), the heat flux at $\hat{t} = 0$ is infinite. As $\hat{t}$ increases, this heat flux decreases monotonically. In contrast, when $\hat{\tau} > 0$, the heat flux at $\hat{t} = 0$ is zero. As $\hat{t}$ increases, the heat flux increases until it attains a maximum value at $\hat{t} \sim O(\hat{\tau})$. For example, for $\hat{\tau} = 0$, 1 and 10, the peak occurs at $\hat{t} \sim 0$, 0.75 and 9. As $\hat{t}$ further increases, the heat flux decreases. For $\hat{t} > \hat{\tau}$, the heat flux associated with the TAC waves with time-delay ($\hat{\tau} > 0$) exceeds that generated by a step change ($\hat{\tau} = 0$). This is because the thermal boundary layer when $\hat{\tau} > 0$ is thinner than it is when $\hat{\tau} = 0$. Also, as $\hat{\tau}$ increases, the fluctuations in the wall heat flux decrease. This reduction in the amplitude of the heat flux fluctuations is commensurate with the reduction in the pressure fluctuations (Fig. 8). For long time, t, the heat fluxes associated with $\hat{\tau} > 0$ and $\hat{\tau} = 0$ approach a common asymptotic value.

Figure 7 depicts the effect of $\hat{\tau}$ on heat flux fluctuations at the cold wall. Because of the small magnitude of the cold wall heat flux, we employed a semi-log scale to illustrate that the fluctuations in the flux persist for $\hat{\tau} > 0$, although their magnitude significantly diminishes as $\hat{\tau}$ increases. As $\hat{t}$ increases, the cold wall heat fluxes for the $\hat{\tau} > 0$ and $\hat{\tau} = 0$ waves approach a common asymptotic value.

In conclusion, the effect of the wall temperature time constant (τ) lasts only for a limited amount of time. For $\hat{t}/\hat{\tau} \gg 1$, TAC waves with $\hat{\tau} > 0$ will behave like TAC waves induced by a step change in the wall temperature ($\tau = 0$).

5. NONLINEAR TAC WAVES

Thus far, we have studied linear waves. The linear approximation is strictly valid only for $A \ll 1$. In this section, we investigate the effect of nonlinearities on the TAC waves' characteristics. To this end, we solve the nonlinear equations with temperature-dependent viscosity and thermal conductivity. In each instance, the adequacy of the temporal and spatial grid spacing is validated by solving the corresponding linear problem and demonstrating that the FD results are virtually identical to the ILT results. We also demonstrate that the FD results are grid-size independent. Finally, we compare our nonlinear solutions to, and obtain an excellent agreement with, recent calculations [10] utilizing wavelet transforms.

Due to the small grid spacing required to achieve the desired accuracy, the numerical calculations were time consuming. Therefore, we restricted the non-

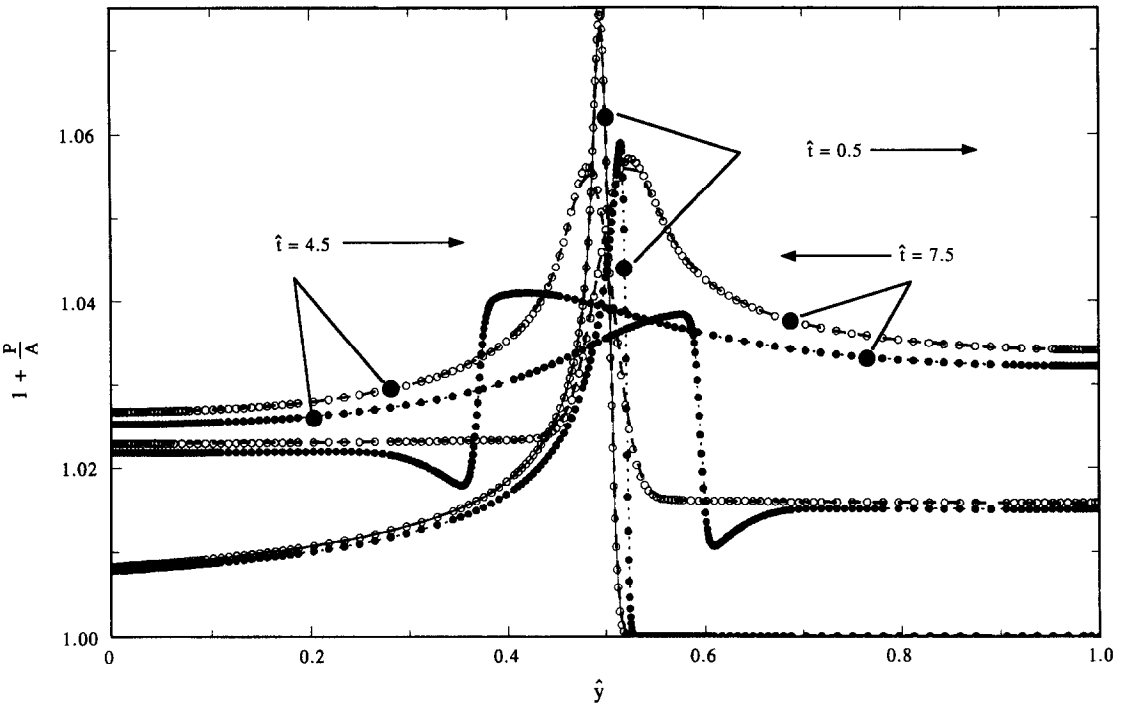

Fig. 9. At times $\hat{t} = 0.5$, 4.5 and 7.5, the linear ILT (solid line), the linear FD (dashed line), the linear wavelet (hollow circles), the nonlinear FD (dotted line), and the nonlinear wavelet (solid circles) pressure waves are depicted as functions of $\hat{y}$. $\tau = 0$. $L = 13\,000$. $A = 1$. The arrows show the direction of the wave motion.

linear simulations to a cavity of length $L = 13\,000$ and to relatively short times.

In the semi-infinite case and for long time periods, nonlinear waves behave like linear ones. This, however, is not true in the case of the confined cavity because the background conditions in the cavity are continuously changing as the hot wall temperature penetrates into the cavity and the average cavity pressure increases.

Figures 1 and 9 compare the behavior of the linear and nonlinear waves for $L = 13\,000$, $A = 1$ and $\hat{\tau} = 0$. More specifically, they depict the linear and nonlinear pressure waves as functions of $\hat{y}$ for various times, $\hat{t}$. The solid (ILT) and heavy dashed (FD) lines correspond to linear waves. The dotted lines correspond to nonlinear waves (FD). The hollow and solid circles (Fig. 9 only) describe, respectively, the linear and nonlinear wavelet solutions [10]. The arrows in Fig. 9 indicate the direction of the wave's motion. Witness the excellent agreement (better than 0.2%) between the ILT and linear FD solutions for $\hat{t} = 0.25$ (Fig. 1) and $\hat{t} = 0.5$ (Fig. 9). There is also very good agreement between the FD (dotted lines) and wavelet (circles) solutions for both the linear (within 2%) and nonlinear waves (within 1%).

The nonlinear waves retain the same characteristic shape as the linear ones—a sharp front followed by a relatively long tail. The nonlinear waves propagate at a slightly higher speed (about 2%) and damp faster (by about 17%) than their linear counterparts. The faster damping of the nonlinear waves may be attributed, in part, to the enhancement of the dissipative mechanisms due to the temperature-dependence of viscosity and thermal diffusivity.

For $\hat{t} > 2$, there is a pressure depression (or rarefaction) downstream of the pressure wave (Fig. 9). At this location, the pressure falls below the background value. This depression is particular to the nonlinear waves, and it is absent in the linear waves.

Next, we examine the effect of the magnitude of the change in the wall temperature (A) on the nonlinear pressure wave. For $\hat{t} = 4.5$ and for $A = 0.2$, 1, 2 and 4, Fig. 10 depicts the linear (solid line) and nonlinear (dotted line) pressure waves as functions of $\hat{y}$. The amplitude of the nonlinear pressure wave is not proportional to A. As A increases, P/A decreases; and the wave speed, the dissipation rate, and the ratio between the pressure dip and the pressure peak increase. We correlated the peak value of the pressure with A using the expression, $p/A = (p/A)_{\text{linear}} \exp(-\bar{\omega}A^{\sigma})$ where both $\bar{\omega}$ and σ are functions of time. For $\hat{t} = 2.5$ and 4.5, we find $\{\sigma, \bar{\omega}\} \sim \{0.85, 0.28\}$ and $\{0.5, 0.064\}$, respectively.

For $A = 1$ and $\hat{t} = 0.5$, 4.5 and 7.5, Fig. 11 depicts the linear (solid line) and nonlinear (dotted line) temperature as a function of $\hat{y}$. For $\hat{t} > 2$, like the pressure wave, the nonlinear temperature wave exhibits a temperature depression (cooling) downstream of the wave front. The temperature depression, like the pressure depression, occurs only in the nonlinear waves. The cooling in front of the wave is caused by the conversion of thermal energy into work. In front of the

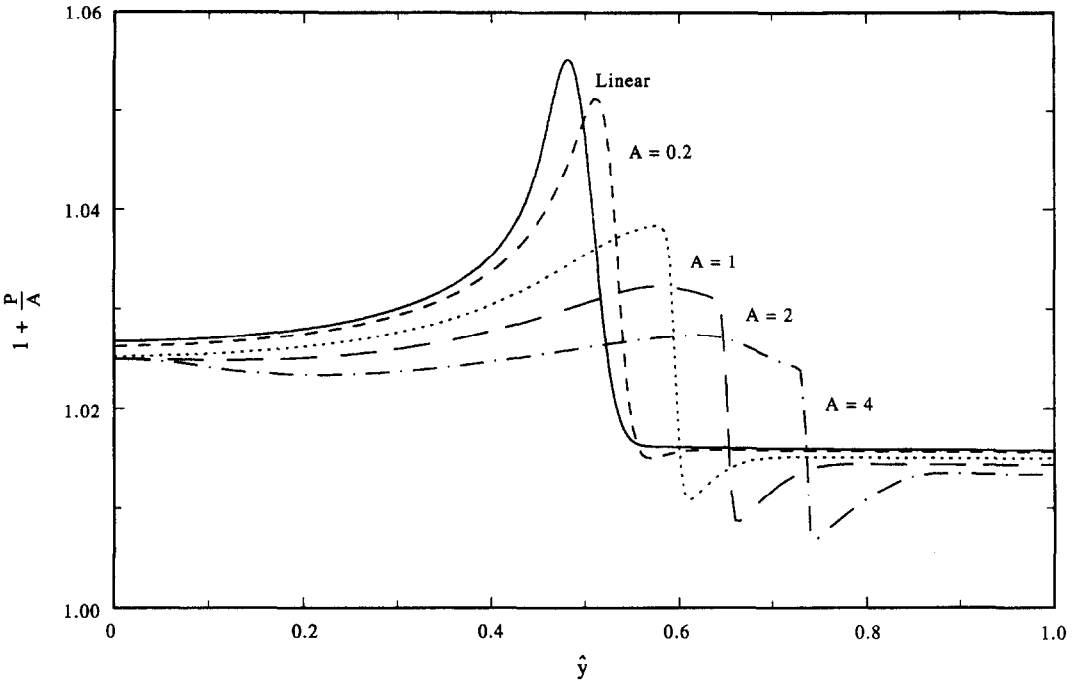

Fig. 10. For $\hat{t} = 4.5$, $A = 0.2$, $A = 1$, $A = 2$ and $A = 4$, the linear (solid line) and nonlinear (dotted line) pressures are depicted as functions of $\hat{y}$. $L = 13\,000$, $\tau = 0$.

wave, the nonlinear work term, $(\gamma - 1)(P+1)(\partial V/\partial y)$, acts as a heat sink. Since $P > 0$, the magnitude of the heat sink is larger in front of the nonlinear waves than it is in front of the linear ones. For this reason, we observe the temperature and pressure depression only in the nonlinear cases.

The temperature field (Fig. 11) exhibits boundary layers at both the hot and cold walls. The hot, nonlinear boundary layer is thicker than the linear one because the gas' thermal diffusivity increases as the temperature increases. This effect of the temperature on the gas' thermophysical properties was not

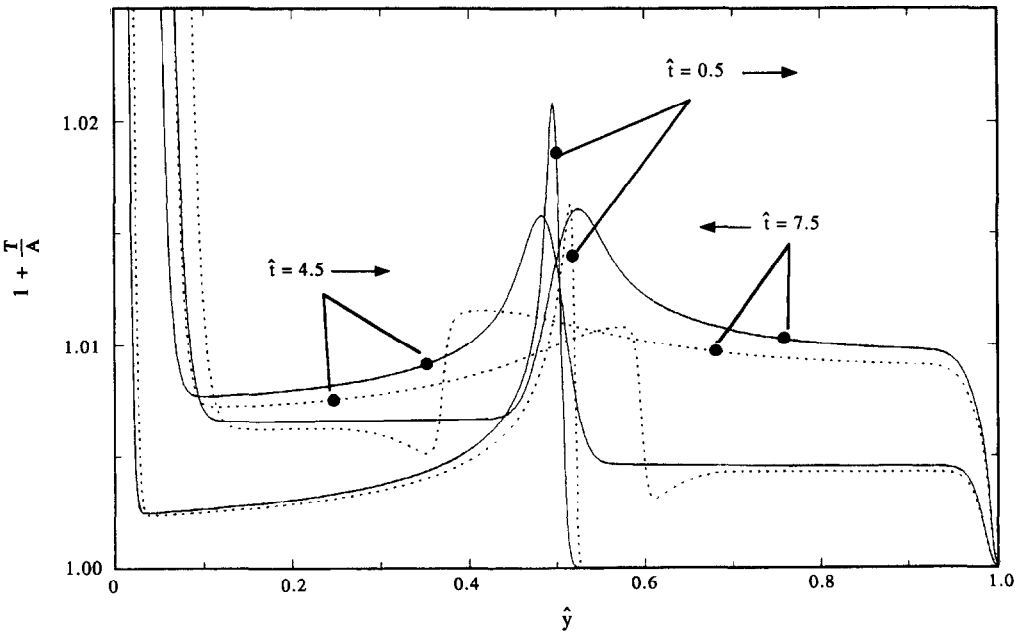

Fig. 11. At times $\hat{t} = 0.5$, 4.5 and 7.5, the linear ILT (solid line) and the nonlinear FD (dotted line) temperature waves are depicted as functions of $\hat{y}$. $\tau = 0$. $L = 13\,000$. $A = 1$. The arrows show the direction of the wave motion.

accounted for in the linear simulations. As a result of the boundary layer thickening, the nonlinear heat flux at the hot wall will eventually become smaller than the linear one (see ref. [13]).

Like the linear wave, the nonlinear wave causes heat flux oscillations similar to the ones depicted in Fig. 7, with the exception that when the temperature depression in front of the nonlinear peak arrives at the wall, the nonlinear wave absorbs heat from the wall.

6. COMPARISON WITH EXPERIMENTS

In this section, we compare our theoretical linear results with Brown's [3] experimental data. Brown used a $L^* = 0.62$ m long ($L = t_0 = 7.8 \cdot 10^6$), 0.02 m i.d., closed, nitrogen filled, plastic tube mounted vertically and heated from below with a thin metal foil supported on a section of fibrous, ceramic insulation. The foil was heated rapidly by a RC circuit and then allowed to cool by heat losses to the environment. The induced pressure wave was measured with a microphone located at a distance of 0.305 m from the foil.

Due to computer power limitations, we were not able to carry out accurate nonlinear calculations for a cavity of the dimensions used in the experiments. Instead, we compared the experimental data with our linear predictions. The computations were carried out for dimensions and a foil temperature history similar to that of the experiment.

Figure 12 depicts the predicted pressure wave (Pa, solid line) at the microphone's location and the foil temperature (dotted line) as functions of time (s). The background pressure increases due to the increase in the average temperature of the cavity. As the foil's temperature decreases, so does the background pressure.

The experimental (rectangles) and theoretical (solid circles) pressure data (in Pa) as a function of time (s) are reproduced in Fig. 13 for $0 < t^* < 0.030$ s. The computed and measured pressure waves have a similar shape, a sharp front and a long 'tail'. The first measured and computed waves are in very close agreement. However, as time increases, the average computed pressure increases much faster than the measured one.

The measured pressure wave also decayed much faster than the computed one. For $t^* > 0.03$ s, the pressure wave is hardly detectable in the experiment, while the theory predicts fairly good size pressure oscillations. The lack of a substantial increase in the background pressure and the faster attenuation of the pressure wave in the experiment can be attributed to the fact that the microphone, which was used to measure pressure, is insensitive to d.c. pressure, to potential gas leakage (the experimental apparatus was not perfectly sealed), to the solid boundaries not being perfectly rigid (and therefore absorbing energy), to the phenomenon not being strictly one-dimensional, and to adverse effects of nonlinearities which become more significant after a few reflections.

In order to eliminate the difference between the background pressures in the experiment and theory, we depicted in Fig. 14 the amplitude (the difference between the highest and lowest pressures) of the experimental (solid circles) and theoretical (open rec-

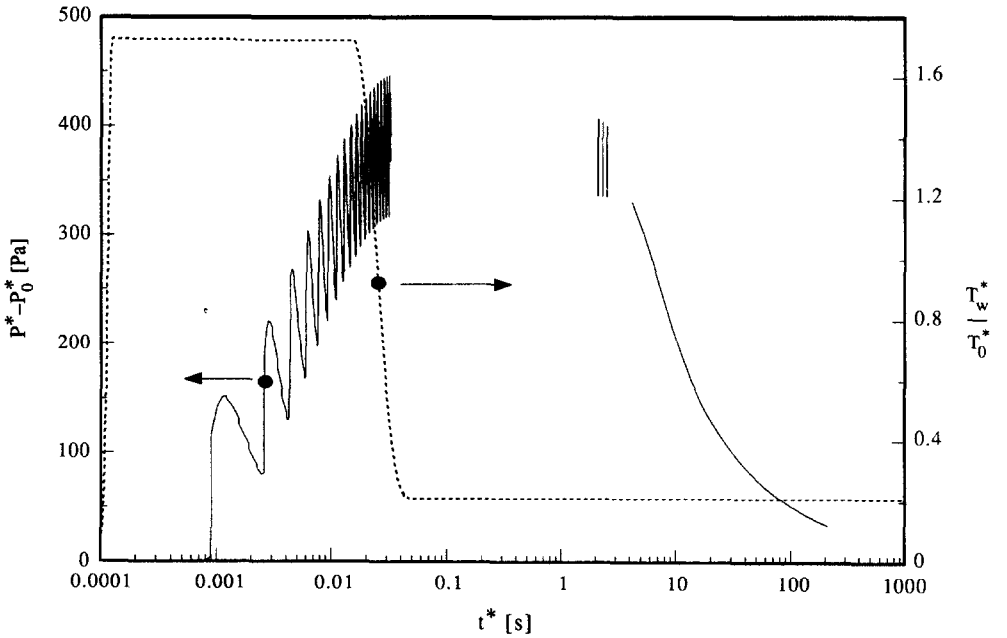

Fig. 12. The pressure wave (Pa, solid line) at the microphone's location and the wall temperature (dotted line) are depicted as functions of time (s).

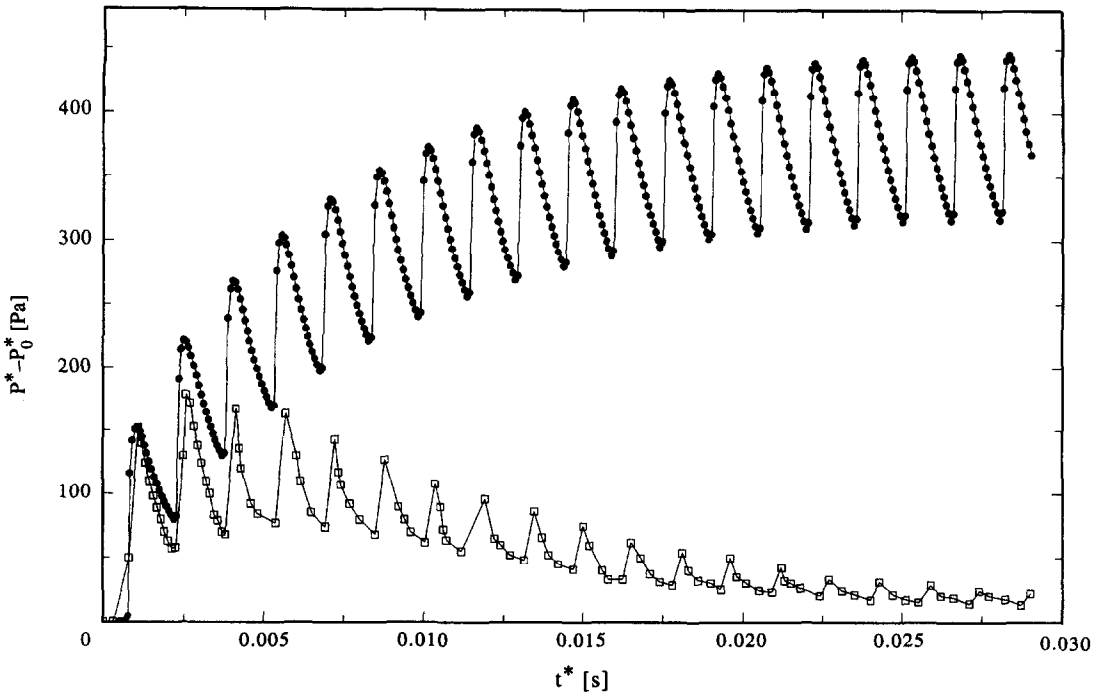

Fig. 13. Comparison of our theoretical predictions with Brown's measurements of the pressure (Pa) detected by the microphone as a function of time (s).

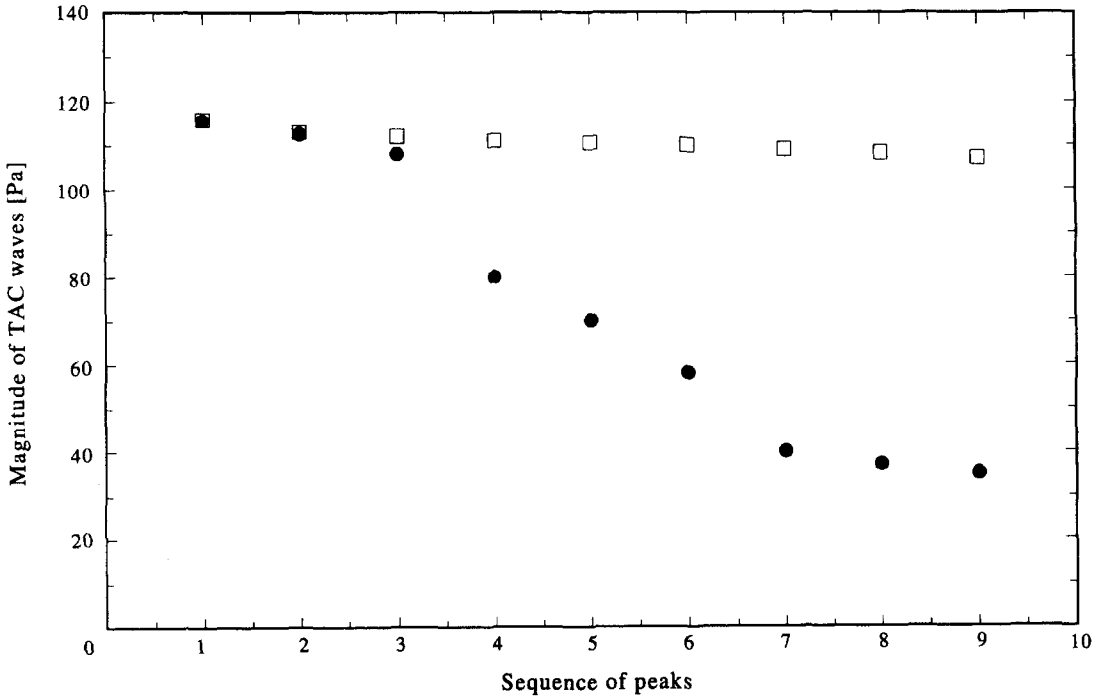

Fig. 14. Comparison of the computed and measured pressure amplitudes as functions of the peak number.

tangles) pressure waves as a function of the peak number. Witness that the first three computed and measured amplitudes have similar values. For the reasons already enumerated, subsequent amplitudes decay much faster in the experiment than in theory.

7. CONCLUSIONS

Using a numerically inverted Laplace transform and a finite difference technique, we studied theoretically one-dimensional linear and nonlinear TAC

wave transmission in a confined region. The linear computations are highly accurate, and they can be used to gauge the adequacy of the grid spacing employed in the nonlinear code. This issue is significant, since it appears that many earlier researchers have selected grid spacings which were too crude to adequately describe the physical phenomena.

Our theoretical results illustrate that linear and nonlinear TAC waves have a characteristic shape consisting of a sharp front and a long tail. These results are in disagreement with virtually all previous numerical works [6–9] which predicted TAC waves having a rounded, symmetric shape about their peaks. However, our results are in excellent agreement with Vasilyev and Paolucci's [10] recent computations, utilizing a novel wavelet transform technique, and they are in good agreement with short time experimental data. The favorable agreement with the experimental data for short times indicates that the mathematical model and the numerical codes employed here are appropriate for modeling the TAC waves.

The short-time behavior of the waves depends strongly on the wall heating rate. As the wall heating time constant (τ) increases, the wave amplitude decreases. For long time periods, $t/\tau \gg 1$, the linear waves induced by gradual and step change wall heating approach a common asymptote.

The nonlinear simulations reveal a rarefaction and temperature depression (cooling) downstream of the wave peak. This phenomenon is not exhibited by the linear waves.

A resonating cavity of the type studied here can be used as an actuator for ultrasonic waves. These waves can be radiated to the ambient, either by using a thin membrane as one of the cavity's walls or by letting some of the waves leak into the environment. The frequency of the waves can be adjusted by varying the cavity's length or by proper selection of the type of gas in the cavity. Such an actuator may be useful for operation under conditions when the more conventional piezoelectric actuators cannot operate or cannot produce sufficiently high amplitude pressure waves.

Finally, the fluctuations in the wall heat flux indicate that the TAC waves can cause high frequency noise in instruments which monitor the power required to maintain an encapsulated probe (i.e. a hot wire or a filament) at a constant temperature.

Acknowledgement—This work was supported, in part, by a grant from the Hewlett-Packard, Little Falls Division. We are grateful to HP's Dr Leonid Blumberg for his support. A part of this paper was presented at the 1993 ASME Winter Annual Meeting (Huang and Bau, [14]).

REFERENCES

1. Y. Huang and H. H. Bau, Thermoacoustic waves in a semi-infinite medium, *Int. J. Heat Mass Transfer* **38,** 1329–1345 (1995).
2. M. Parang and A. Salah-Eddine, Thermoacoustic convection heat-transfer phenomena, *AIAA J.* **22,** 1020–1022 (1984).
3. M. A. Brown, Thermally induced pressure wave in a gas : experimental observation and theoretical prediction of thermoacoustic convection, Ph.D. thesis, University of Pennsylvania, Philadelphia, PA (1992).
4. M. A. Brown and S. W. Churchill, Transient behavior of an impulsively heated fluid, *Chem. Engng Technol.* **16,** 82–88 (1993).
5. M. A. Brown and S. W. Churchill, Experimental measurements of pressure waves generated in a confined gas by impulsive heating of a surface. *AIChE J.* **41,** 205–213 (1995).
6. B. K. Larkin, Heat flow to a confined fluid in zero gravity, *Prog. Astro. Aeronaut.* **20,** 819–832 (1967).
7. L. W. Spradley and S. W. Churchill, Pressure and buoyancy driven thermal convection in a rectangular enclosure, *J. Fluid Mech.* **70,** 705–720 (1975).
8. H. Ozoe, N. Sato and S. W. Churchill, The effect of various parameters on thermoacoustic convection, *Chem. Engng Commun.* **5,** 203–221 (1980).
9. H. Ozoe, N. Sato and S. W. Churchill, Numerical analyses of two and three dimensional thermoacoustic convection generated by a transient step in the temperature of one wall, *Numer. Heat Transfer A* **18,** 1–15 (1990).
10. O. V. Vasilyev and S. Paolucci, A dynamically adaptive multilevel wavelet collocation method for solving partial differential equations in a finite domain, *J. Comput. Phys.* **125,** 498–512 (1996).
11. R. Piessens and R. Huysmans, Automatic numerical inversion of the laplace transform, *ACM Trans. Math. Software* **10,** 348–353 (1984).
12. C. A. J. Fletcher, *Computational Techniques for Fluid Mechanics*, Vol. 1, pp. 278–279. Springer, Berlin (1991).
13. Y. Huang, Transport processes in thermal conductivity detectors, Ph.D. dissertation, University of Pennsylvania, Philadelphia, PA (1995).
14. Y. Huang and H. H. Bau, Thermoacoustic convection. In *Heat Transfer in Microgravity* (Edited by C. T. Avedisian and V. A. Arpaci), Vol. ASME HTD-269, pp. 13–22. ASME, New York (1993).